Redundant Integrated Flight-Control/Navigation Inertial Sensor Complex

R.E. Ebner* and J.G. Mark*
Litton Systems, Inc., Woodland Hills, Calif.

The preliminary design of a redundant strapdown navigation system for integrated flight-control/navigation use is presented. Based on tuned-gimbal gyros, a compact configuration (13 in. × 13 in. × 14 in.) has been achieved for fail-operational/fail-operational redundancy. Hardware and software design of a four-channel system configuration is given. The system consists of four gyros, eight accelerometers, and four processors. Compact packaging into four identical chassis is based on the symmetry properties of an octahedron. The design matrix for least-squares combinations of *n* two-degree-of-freedom gyros is derived, and general parity equations are shown for extracting errors from measurements. A limitation on the amount of sensed information for failure isolation of some second-gyro failures is described, and system failure probability is calculated from hardware failure rate, channel interconnection, and signal-to-noise ratio. Test data are presented for skewed, dual-redundant strapdown inertial measurement units, including typical parity equation responses during physical motion, simulated gyro and accelerometer failures, and a 180-deg turn with a 20-deg roll angle. Fault detection and isolation time for various failure amplitudes and likelihood of false alarms for the assumed error detection amplitudes are given.

Nomenclature

CARSRA	= computer aided redundant system reliability analysis
CCV	= control configured vehicle
CEP	= circular error probable
FBW	= fly-by-wire
FCS	= flight control system
FDI	= failure detection and isolation
fo-fo	= fail-operative/fail-operative
GP	= general purpose
IMU	= inertial measurement unit
INS	= inertial navigation system
I/O	= input or output
KOP	= thousand operations per second
LRU	= line replaceable unit
MTBF	= mean time between failures
RM	= redundancy management
SAS	= stability augmentation system
Scorsby	= three-axis sinusoidal angular motion
SDF	= single degree of freedom
TDF	= two degrees of freedom
VTOL	= vertical takeoff and landing aircraft

Introduction

APPLICATION of strapdown inertial sensors that are shared between flight control systems and navigation needs has been suggested for cost reduction of future aircraft avionics, both commercial and military. The flight safety requirements of high-authority flight control systems of projected aircraft, however, emphasize the need for redundant avionics elements. Design of such equipment must be highly efficient in order that cost-saving potentials may be realized.

This paper documents work performed by Litton for the preliminary design of a redundant strapdown inertial navigation unit,[1] plus subsequent concept demonstration testing. The preliminary design and demonstration tests used previously developed tuned-gimbal gyroscopes, since they are closer to a production configuration than laser gyros. Some of the general techniques and conclusions are applicable to ring laser gyros when they become generally available.

Received June 16, 1977; presented as Paper 77-1109 at the AIAA Guidance and Control Conference, Hollywood, Fla., Aug. 8-10, 1977 (in bound volume of Conference papers); revision received Sept. 16, 1977. Copyright © American Institute of Aeronautics and Astronautics, Inc., 1977. All rights reserved.

Index categories: Sensor Systems; Guidance and Control; Spacecraft Navigation, Guidance, and Flight-Path Control.

*Member of the Senior Technical Staff.

Applications

Redundancy and reliability requirements for a flight-control sensor complex are a function of the flight control modes employed plus the natural stability of the airframe. Table 1 illustrates the growing importance of redundant inertial data as SAS, CCV, autoland, and improved handling modes are applied to the aircraft FCS. The equipment described in this paper applies to the more demanding vehicles, such as VTOL and CCV, where redundancy is required for most inertial functions. Then, an integrated set of inertial sensors with self-contained redundant preprocessing can prove very cost-effective over separate, redundant rate, attitude, and navigation sensors.

Table 1 Inertial data redundancy requirements vs application

Redundant Inertial Data	Conventional Aircraft	FCS Yaw SAS	3-Axis SAS, FBW, CCV	Autoland, VTOL, Reduced Pilot Workload	All-Weather VTOL
Attitude/Heading	X	X	X	X	X
Yaw Rate		X	X	X	X
Pitch/Roll Rates			X	X	X
Body Acceleration			X	X	X
Ground Speed/Track				X	X
Position Coordinates					X

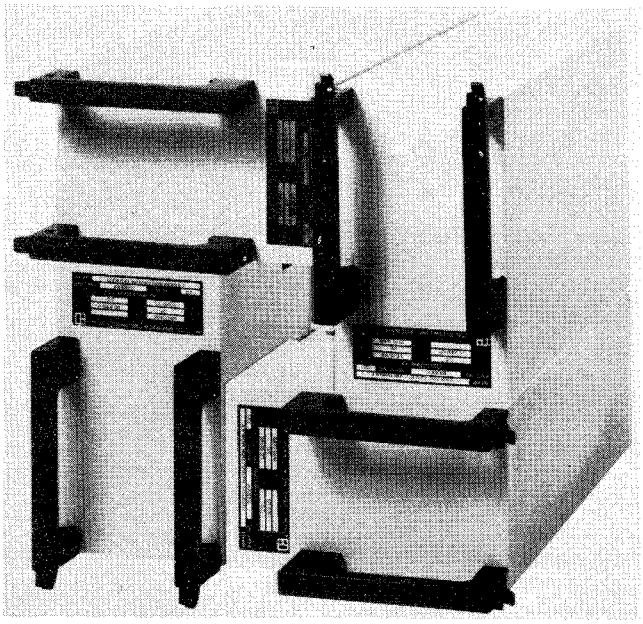

Fig. 1 Mock-up of the redundant strapdown inertial navigation system.

System Description

The fo-fo navigator designed to meet Ref. 1 requirements was configured to consist of four interchangeable plug-in units. Each unit contains one of the redundant channels of hardware consisting of a TDF tuned-gimbal gyroscope, two linear accelerometers, a computer with I/O, and a power supply. The gyro/accelerometer axes are skewed within each chassis so that when the four channels are installed, as in Fig. 1, the four gyro and eight accelerometer axes are distributed in space. This insures that normal operation continues regardless of which two sensors fail. Accurate interchannel alignment is maintained by the aircraft mounting provisions. For applications requiring physical separation of units, channels may be separated by pairs. If significant aircraft flexure occurs between pair locations, however, redundancy management performance of attitude, heading, velocity, and navigation outputs would degrade.

A simplified system block diagram is shown in Fig. 2. Each channel consists of: one TDF gyro with pulse rebalance electronics, two accelerometers with pulse rebalance electronics, one GP digital computer, external I/O,† internal and intercomputer I/O, and power supply.

The amount of cross-strapping between channels has been minimized for reduced cost. Inertial instrument data are transferred to other channels after computer processing; power supplies affect only one channel. Interchannel I/O and software synchronizaton are provided for sensor redundancy comparisons and to allow selection of sensors for further processing.

The system characteristics are summarized in Table 2. Values are approximate, especially in the area of computer requirements, navigation accuracy, and thus system cost, since they are a function of specific user requirements. Some increase in weight and volume may be expected in a more demanding thermal environment requiring highly efficient heat exchangers rather than impingement cooling.

Least-Squares Design Matrix for TDF Gyro

The array of four nonorthogonal TDF gyros contains adequate information to derive the three orthogonal axes of vehicle rate in aircraft axes. Redundant measurement data are

†It is assumed that using avionics will perform additional voting functions.

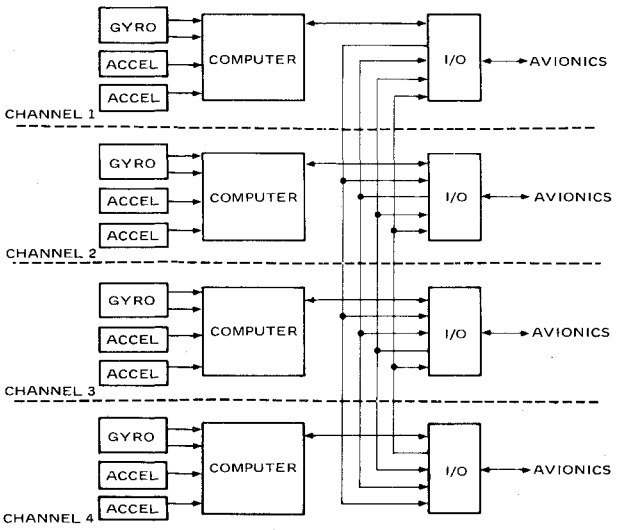

Fig. 2 Simplified system block diagram.

available if the outputs of two or more gyros are combined, and it is often desirable to combine these outputs using equations which minimize instrument errors in a least-squares fashion. Design equations are thus now derived for n TDF gyros having $2n$ outputs using a unique matrix operator, termed a projection matrix, which greatly simplifies mathematical manipulation of TDF variables.

The total angular rate of the instrument cluster is represented by the vector ω. Also the unit vector $\hat{S}_i$ is assumed to coincide with the spin vector of the ith gyro and ω_i is the projection of ω on a plane normal to $\hat{S}_i$ (see Fig. 3). Thus ω_i is the angular rate vector as measured by an ideal ith TDF gyro. In vector notation, the relationship between ω and ω_i is:

$$\omega_i = \omega - \hat{S}_i(\hat{S}_i \cdot \omega) \tag{1}$$

It is more convenient, however, to express this relationship in terms of a projection matrix

$$\omega_i = [P_i]\omega; \quad [P_i] = [I - \hat{S}_i \cdot \hat{S}_i^T] \tag{2}$$

Thus, $[P_i]$ is a matrix which projects ω onto a plane normal to $\hat{S}_i$. Similar relationships may be written for each of the n TDF gyros of the instrument cluster. Thus,

$$\begin{aligned} \omega_1 &= [P_1]\omega \\ \omega_2 &= [P_2]\omega \\ &\cdot \\ &\cdot \\ \omega_n &= [P_n]\omega \end{aligned} \tag{3}$$

Equation (3) may also be written as:

$$\begin{bmatrix} \omega_1 \\ \omega_2 \\ \cdot \\ \cdot \\ \omega_n \end{bmatrix} = \begin{bmatrix} P_1 \\ P_2 \\ \cdot \\ \cdot \\ P_n \end{bmatrix} \omega \quad \text{or } \tilde{\omega} = [A]\omega \tag{4}$$

where $\tilde{\omega}$ is a $3n$ vector and $[A]$ is a $3n \times 3$ matrix.

Assuming that the spin axes of at least two of the n gyros are not colinear, it is possible to solve Eq. (4) for the input rate ω in a variety of ways. In this approach a least-squares

Table 2 Summary of system characteristics

Size[a]	13 × 13 × 14 in.
Weight[a]	61 lb
Power	540 W
LRUs	4 identical channels
Redundancy	fail-op/fail-op
Failure probability (3 h)[a]	less than 10^{-8}
Gyros	
type	G-6/7 tuned rotor
quantity	4
Accelerometers	
type	A-1000
quantity	8
Computer (1 of 4)	150 KOP, 8K-words memory
Outputs	Angular rates, accel, attitude, heading, velocity, position
Inertial nav accuracy	1-10 nm/h
Cost, system	$100,000-180,000

[a] Commercial version.

regression method is used, viz:

$$\langle\omega\rangle = [A^T A]^{-1}[A]^T\tilde{\omega} \tag{5}$$

where $\langle\omega\rangle$ indicates the least-squares estimate of the input rate ω. This computation may be simplified by first considering the matrix $[A^T A]$, and, using the definition of $[A]$ in Eq. (4), it follows that

$$[A^T A] = \sum_{i=1}^{n} [P_i]^T [P_i] \tag{6}$$

Since each $[P_i]$ is a projection matrix,

$$[P_i]^T = [P_i] \text{ and } [P_i]^2 = [P_i] \tag{7}$$

the matrix $[A^T A]$ simplifies to

Then,

the sum of the individual projection matrices. Now consider $[A]^T$ operating on $\tilde{\omega}$. Since ω_i is already the projection of ω on a plane normal to S_i,

$$[P_i]^T\omega_i = [P_i]\omega_i = \omega_i \tag{9}$$

Then

$$[A]^T\tilde{\omega} = \sum_{1}^{n} [P_i]^T\omega_i = \sum \omega_i \tag{10}$$

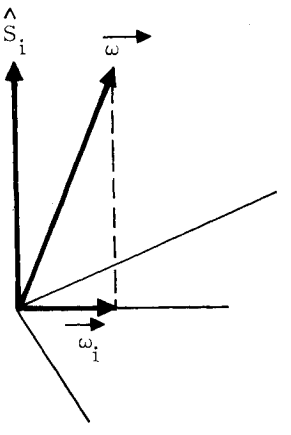

Fig. 3 Illustration of TDF gyro sensing vector, ω_i.

Using the results obtained in Eqs. (8) and (10), Eq. (5) may be rewritten as:

$$\langle\omega\rangle = \left[\sum_{i=1}^{n} P_i\right]^{-1} \sum_{i=1}^{n} \omega_i \tag{11}$$

It is convenient to introduce a matrix $[D]$, referred to as a design matrix, such that

$$[D] = \left[\sum_{i=1}^{n} P_i\right]^{-1} \tag{12}$$

and rewrite Eq. (11) as

$$\langle\omega\rangle = [D] \sum_{i=1}^{n} \omega_i \tag{13}$$

Clearly, under the assumption that at least two of the gyro spin axes are not colinear, $[D]$ exists and can be easily computed for a particular cluster configuration from the definition of the projection matrices, Eq. (2). Further, in this formulation $[D]$ weights the outputs of the individual instruments so that the sum of the squares of the errors associated with all of the instrument axes is minimized.

Parity Equations and Geometry

The formulation of parity equations‡ for TDF instruments is inherently different from the formulation for SDF instruments. In the TDF case, the output of only two instruments is required to form a parity equation. The four components of rate information available from the two TDF instruments are insufficient to allow detection of all possible instrument failures as with four SDF instruments, since there is a significant probability of dual-axis, gyro failure modes.

For two TDF gyros (say i and j) whose spin axes are not colinear, a single parity equation T_{ij} may be formed by comparing the gyro outputs along a direction normal to the gyro spin axes S_i and S_j:

$$\hat{e}_{ij} = (\hat{S}_i \times \hat{S}_j) / |\hat{S}_i \times \hat{S}_j|$$

$$T_{ij} = (\omega_i - \omega_j) \cdot \hat{e}_{ij}$$

For an ensemble of n TDF gyros, no two of whose spin axes are colinear, a set of $(n-1)!$ independent parity equation can be formed by letting $1 \le i < j \le n$. While in reality the parity equations cannot directly represent angular rates but must be filtered to minimize the effects of "noise," the failures of most $n-1$ gyros can be detected, and at most $n-2$ failures can be isolated by comparing the absolute value of the filtered T_{ij}'s to some threshold value.

The selected system configuration consists of four TDF gyros and eight SDF accelerometers. No two gyro input axes or spin axes are coincident for fail-op/fail-op capability. Eight accelerometers are used, also none coincident, to allow the highly maintainable packaging approach previously described, even though only six would have been sufficient for dual-failure isolation. The instrument axes are distributed evenly in space in order that performance degradation with two failures is uniform and minimum, regardless of which two instruments fail first.

Figure 4 shows the selected gyro and accelerometer geometry. The spin axes S are normal to faces of half of an octahedron. The gyro sensitive axes, x and y, lie in each face, and accelerometer axes are coincident with them. Note that gyro 1 can be oriented along gyro 2 by rotating 90 deg about the x_B (roll) axis, etc. This symmetry provides the compact

‡Equations which combine redundant measurements of the same physical quantity in such a way as to remove the quantity being measured, thus exposing the combined measurement error.

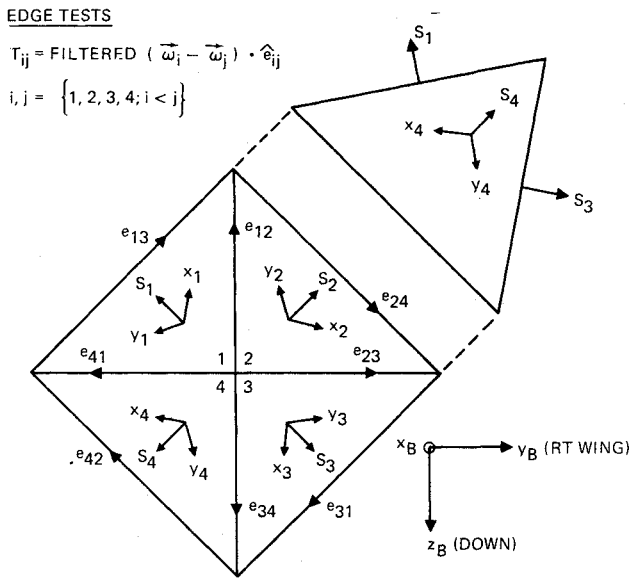

Fig. 4 Semioctahedral gyro-axis orientation.

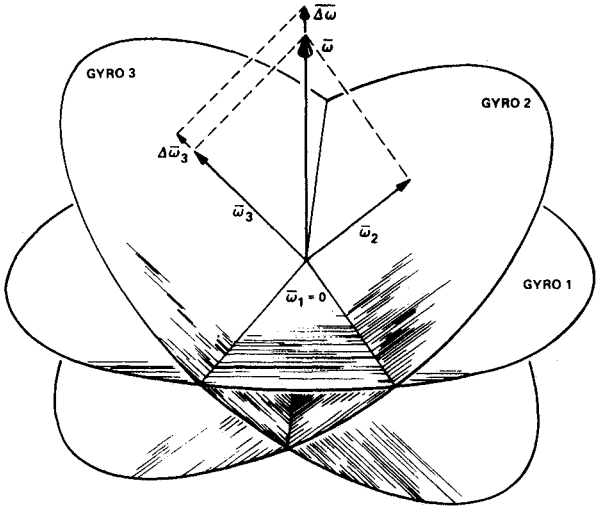

Fig. 5 Illustration of three-gyro isolation singularity.

packaging arrangement shown in Fig. 1, where each of the four channels is installed with a 90-deg rotation relative to the adjacent one.

Six unique parity equations T_{ij} are thus available as shown in Fig. 4. If two or more equations involving a specific gyro indicate an error condition, that gyro is classified as failed. After one gyro failure, only three equations remain. The two-or-more criterion still applies, however.

Processing of a parity equation involves an imperfect integration. For extremely small, nonfailure gyro drift errors, the output remains below the error detection threshold. The threshold may thus be kept constant as a function of time. For large drift errors, the output is essentially an angle or, in the case of accelerometers, a velocity. Thus, angular and linear transients to the flight control system during failure modes can be kept below a desired level.

Three TDF-Gyro FDI Singularity

Four noncoincident TDF gyros contain more than sufficient measurement information for complete, self-contained detection and isolation of a two-axis gyro failure. Following a first gyro failure, a second two-axis gyro failure can easily be detected using the remaining parity equations. There are certain low-probability two-axis failure modes, however,

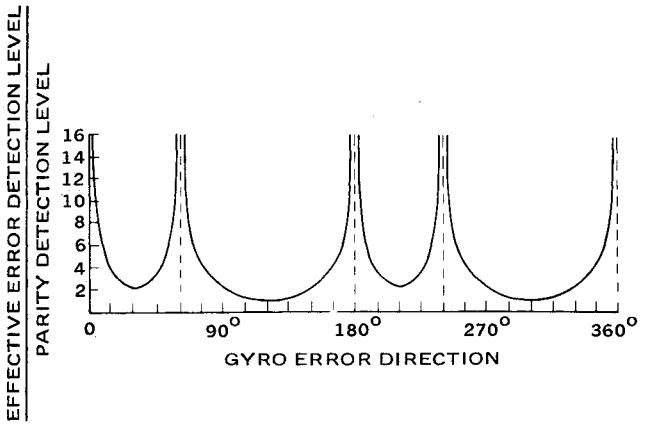

Fig. 6 Ratio of effective detection level to parity detection level vs direction of gyro error.

where the failed gyro cannot be isolated. These isolation singularities will now be described, beginning with a proof of their existence.

Consider three gyros, the sensitive axes of each represented by a plane surface. The orientation of the two gyro input axes in this plane is immaterial, since measurements made in one orientation can be changed to another with a simple coordinate transformation about the spin axis.

Consider next a vehicle angular rate $\bar{\omega}$ along the spin axis of gyro 1 of Fig. 5. The rates sensed by each gyro are the projections of $\bar{\omega}$ onto each measurement plane, where $\bar{\omega}_1 = 0$.

Given the gyro measurements $\bar{\omega}_2$ and $\bar{\omega}_3$, one can reconstruct an estimate of $\bar{\omega}$ along the intersection of two planes—one plane is normal to gyro measurement plane 2 and along $\bar{\omega}_2$, the other plane is normal to gyro measurement plane 3 and along $\bar{\omega}_3$. This reconstructed ω is also consistent with $\omega_1 = 0$.

If gyro 3 has an error $\Delta\bar{\omega}_3$ along the direction of $\bar{\omega}_3$, the error in the reconstructed $\bar{\omega}$, $\Delta\omega$, is along the direction of $\bar{\omega}$. The same error could have been caused by an error in gyro 2 along the direction of $\bar{\omega}_2$. Gyro 1 cannot contribute information in determining whether $\Delta\omega$ was caused by gyro 1 or gyro 2 since $\Delta\omega$ is normal to its measurement plane. Therefore, isolation singularities occur in each gyro measurement plane for gyro drift errors along the projections of the other gyro spin axes onto that plane.

This isolation singularity may also be observed in parity equations. Each parity equation is processed to determine if errors exceed some predetermined level. If the vector direction of a gyro drift is along the test direction of the parity equation, the actual error detection level in gyro axes is the same amplitude as the parity detection level. If the gyro drift direction is displaced from the parity equation test direction, it takes a higher gyro drift to exceed the parity detection level.

This geometrical amplification of parity detection level as a function of gyro error direction is illustrated in Fig. 6. This figure is based upon the octahedron geometry of Fig. 4, with one gyro previously failed. The isolation singularities, where effective error detection level is infinite, are clearly shown. If the parity detection level is set at the noise level of the gyro, the curve of Fig. 6 is a noise vs direction boundary, below which failures cannot be isolated.

If there is a system requirement that system failure occurs for nonrecoverable gyro errors above some level, a portion of gyro failures will cause system failure. If large errors are allowed, relative to the nominal gyro noise level, the probability of nonisolatable failure modes is extremely small. This is illustrated in Fig. 7, which contains polar plots of Fig. 6 with the addition of circles representing gyro error amplitudes which could cause system failure. For very large failure levels such as would be allowed by the flight control system (compared with inertial-grade gyro noise), only a very

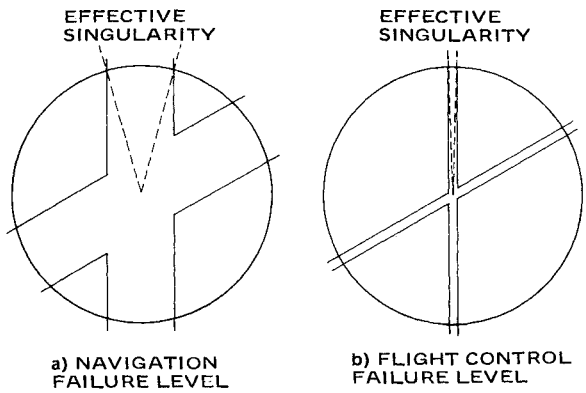

Fig. 7 Polar plots of gyro failure amplitude vs failure direction.

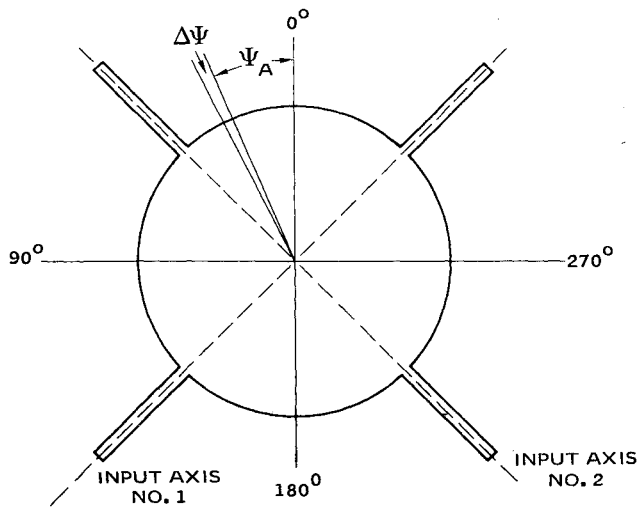

Fig. 8 Hypothetical plot of failure probability density ($P/\Delta\psi$) vs failure direction (polar coordinates).

small portion of the failure circle is inside of the effective isolation noise boundary.

The actual statistical nature of strapdown TDF gyro failure modes as a function of amplitude and direction is not available. In general, a higher failure probability is expected along a torquer axis than a two-axis failure with some predetermined direction. This is illustrated in Fig. 8. If ψ_A is the angle at which an isolation singularity occurs and $\Delta\psi$ is the effective width of the singularity, for small values of $\Delta\psi$ the probability of a failure along ψ_A is smaller than the probability of a failure along an input axis. Therefore, input axes should not be oriented along a potential isolation singularity.

Computer Mechanization

The four-channel computer mechanization which has been selected is shown in Fig. 9. Following compensation of the channel's local instruments for constant error coefficients, measurements are cross-fed between computers. Each computer then performs FDI/RM to select instruments to be used for subsequent calculations. Table 3 shows instrument

Table 3 Gyro pair selection vs failure indication

Chan 0	1	2	3	4	1/2	1/3	1/4	2/3	2/4	3/4
1	1,2	1,2	1,3	1,2	1,2	1,3	1,2	1,2	1,4	1,3	1,2
2	2,3	2,3	2,3	2,4	2,3	2,3	2,4	2,3	2,4	2,3	2,1
3	3,4	3,4	3,4	3,4	3,1	3,4	3,4	3,2	3,4	3,1	3,1
4	4,1	4,2	4,1	4,1	4,1	4,3	4,2	4,2	4,1	4,1	4,1

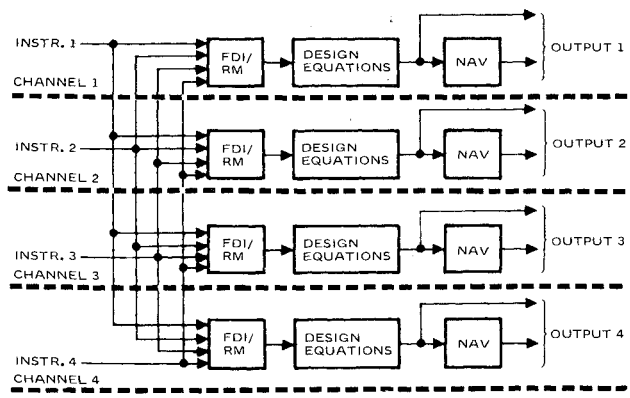

Fig. 9 Four-channel software mechanization.

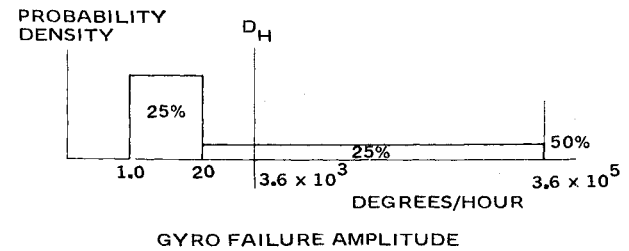

Fig. 10 Assumed distribution of gyro failures as a function of failure amplitude.

selection logic based on FDI failure indications where each channel uses a different pair of gyros. The advantages of this approach are that 1) error buildups which occur during FDI in one or two channels may be eliminated by resetting to a known-unaffected channel, and 2) very small drifts, inside of FDI thresholds, can be detected and isolated by reference to external data such as position updates or terminal error, for subsequent maintenance action.

Requirements for strapdown navigation are not unusual in the redundant implementation. Computer requirements are for a computational speed of approximately 150 KOPS and a memory of 8K words. Of the total, only about 10% of the speed is due to FDI/RM which indicates the excellent cost-effectiveness of the approach.

System Failure Probability

The probability of system failure depends upon the basic component failure rates, redundant element interconnections, and the probability of recovering from each failure condition through FDI (coverage). Two failure rates have been calculated, one for commercial environments with a channel MTBF of 4000 h, and the other for more extreme environments with a channel MTBF of 2000 h. This latter quantity is equivalent to a full INS MTBF of 1600 h, by adding one gyro and one accelerometer.

The redundant element interconnection is shown in Fig. 2. The coverage for any first failure condition is assumed to be unity, as is coverage for a second accelerometer pair, computer, or power supply failure.

Coverage for the second gyro failure is based upon 50% effective self-test with the remaining, soft failures distributed with amplitude as shown in Fig. 10. Half of soft failures are assumed under 20 deg/h since more failure modes are applicable. All gyro failures are assumed to involve two axes, with the vector direction of the error independent of amplitude and with a uniform probability distribution over 360 deg. Normal gyro drift noise is assumed to be 0.1 deg/h.

At any given failure amplitude, the percentage of second gyro failures which cannot be isolated for failure recovery is proportional to normal gyro noise and inversely proportional to failure amplitude (Fig. 7). Using this property and in-

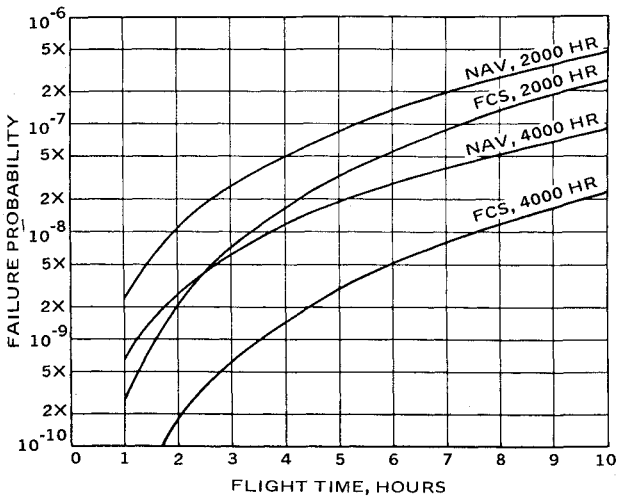

Fig. 11 System failure probability vs flight duration.

tegrating a variable percentage of failure amplitude probability density (Fig. 10) over the range of interest leads to the probability of ambiguity. Application of a self-test percentage of 50% then leads to a coverage of 0.99 for a 1 deg/h minimum failure level and 0.999999 for 1 deg/s minimum failure level. System attitude and navigation failure (NAV) is assumed to occur if gyro error exceeds 1 deg/h. Angle rate output failure (FCS) is assumed to occur if gyro error exceeds 1 deg/s.

Figure 11 shows the probability of exceeding these two performance levels (NAV and FCS) without recovery, i.e., the system fails, as a function of channel MTBF and flight time. Calculations were made using the CARSRA computer program described in Ref. 2.

Failure probability can be significantly decreased for flight control modes by cross-strapping sensor data into all four computers insteady of only one. Slightly higher channel costs result from this more flexible I/O. However, because of the dependence of flight safety on these outputs, the added cost is probably warranted for long flight-duration applications.

Applications requiring only fail operative redundancy due, for exmple, to the availability of direct manual flight control modes could employ only three of the channels for reduced cost. Assuming that the four-channel geometry is retained, the geometry is less than optimum for three. Performance degradation is slight, however, and having expansion capability to four may be desirable, especially during early program phases or in lieu of onboard spares.

Test Results

Litton flight-tested its strapdown system, the LN-50, in the company's Swearingin/Merlin turboprop aircraft during 1976. Various flight profiles were flown to ascertain system sensitivities, including aerobatic maneuvers within the Merlin flight envelope. Performance achieved over 14 flights was better than 1 naut mile/h, CEP, as shown in Ref. 3. Gyro noise of 0.5 arc-s (1σ) was achieved with this hardware, at a data sampling rate of 128 Hz. In addition, gyro bandwidth was 80 Hz, strongly suggesting the applicability of these gyro outputs to flight control rate sensing requirements. Accelerometer noise and bandwidth were 0.0015 ft/s (1σ) and several hundred Hz, respectively, well within FCS needs.

A redundant sensor version of the LN-50 has been tested, demonstrating the skewed-instrument redundancy management techniques developed on the Ref. 1 study. Two orthogonal inertial measurement units (IMUs) containing two TDF gyros and three SDF accelerometers each, are mounted to a common plate with one of them skewed. The four gyro spin axes are uniformly distributed about a 90 deg cone. Normal operation can be achieved using any pair of gyros, thus demonstrating fo-fo capability.

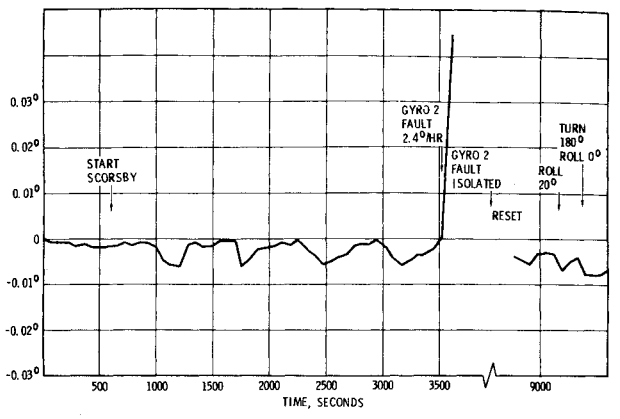

Fig. 12 Gyro parity equation; I_{12}, 3 deg, 0.1 Hz three-axis Scorsby.

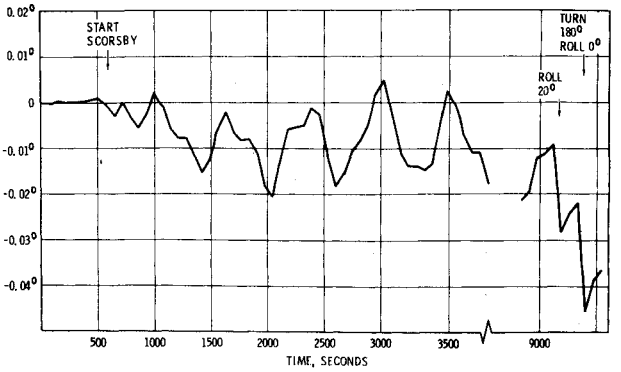

Fig. 13 Gyro parity equation, I_{14}; 3 deg, 0.1 Hz three-axis Scorsby.

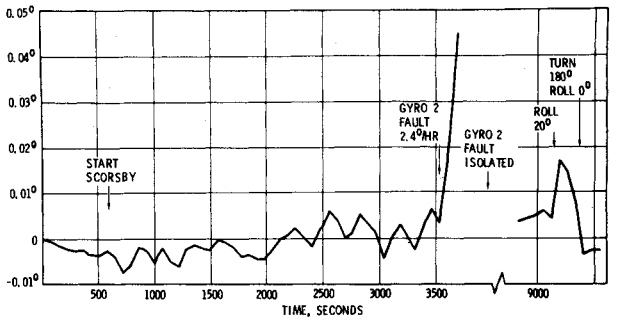

Fig. 14 Gyro parity equation; I_{24}, 3 deg, 0.1 Hz three-axis Scorsby.

The digital computer is programmed to perform two complete navigation solutions simultaneously. One solution uses the nominal IMU with no simulated instrument failures and forms a reference. The second solution can operate with any other pair of gyros or set of accelerometers, selected either manually or automatically by FDI logic.

Simulated instrument failures may be entered into the computer through the control/display unit as biases. Gyro and accelerometer parity equations are solved and filtered to detect these bias failures. FDI logic is then included to isolate the failed instrument and select the new instrument sets.

For laboratory testing the dual-skewed IMU plate was attached to a three-axis motion simulator. Thus, failure detection, isolation, system reconfiguration, and navigation could be performed during controlled motion conditions to determine the likelihood of false alarms or missed alarms.

Figures 12-16 show data recorded during the demonstration. Integrated gyro parity equations I_{12}, I_{14}, and I_{24} are shown during static operation, Scorsby motion, and a simulated aircraft turn. I_{13}, I_{23}, and I_{34} are similar in form. Scorsby motion is apparent in the plots as a low, beat-frequency between the 10-s motion period and the 70-s data

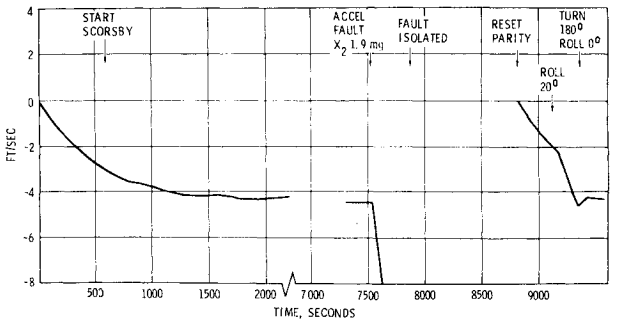

Fig. 15 Accelerometer parity equation; I_3, 3 deg, 0.1 Hz three-axis Scorsby.

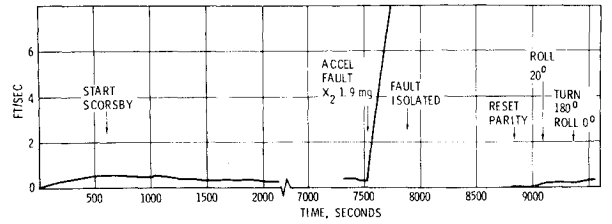

Fig. 16 Accelerometer parity equation; I_4, 3 deg, 0.1 Hz three-axis Scorsby.

sampling period. Greater coupling occurs in I_{14} since the IMU-to-IMU alignment was only accurate to approximately 0.1 deg in azimuth. Gyros 1 and 2 are in the level IMU, 3 and 4 in the skewed IMU.

Introduction of a simulated gyro 2 failure of 2.4 deg/h causes rapid divergence of I_{12} and I_{24}, and when the detection level of 0.1 deg is reached in both equations, failure isolation is accomplished. Isolation of the failed gyro occurred in 420 s. A large simulated fault of 1.4 deg/s was isolated in 0.14 s. If IMU-to-IMU azimuth alignment were better, the error detection threshold can be lowered to 0.05 deg or less, reducing fault isolation times by approximately a factor of 2. An integrator time-constant of 512 s produces a minimum detectable drift of 1 deg/h. Different processing will be needed for detection and isolation of small drifts affecting navigation performance.

The aircraft turn, simulated by entering a 20-deg roll angle into the table, rotating about yaw 180 deg, then returning roll to 0 deg, induced some errors into the integrated parity equations. The primary cause is again the IMU-to-IMU azimuth misalignment, which is correctable.

Two of the nine accelerometer integrated parity equations are shown in the figures. A full set of 15 equations was not available due to the use of standard orthogonal IMUs. Two sets of three accelerometers lie in two orthogonal planes and out-of-plane measurements cancel out of the parity equations involving each of these sets. Full fo-fo capability is thus not achieved with six accelerometers.

Coupling of Scorsby motions into accelerometer parity is very slight. For an 8 ft/s detection threshold and a 512-s integrator time-constant, a 0.5-mg bias is the minimum detectable level. IMU-to-IMU alignments were performed to approximately 50 arc-s. A simulated accelerometer failure of 1.9 mg was isolated in 354 s. A 0.12-g fault was isolated in 4 s. Again some errors occurred during the simulated turn, primarily due to azimuth IMU-to-IMU misalignment.

Conclusions

A compact redundant inertial sensor system configuration is described where outputs can be maintained in the presence of any two failures. Only four TDF tuned-gimbal gyroscopes are required, the fail-operative, fail-operative capability being achieved by skewing the gyros with spin axes perpendicular to nonparallel faces of an octahedron. Eight SDF linear accelerometers and four digital computers are also employed, with all equipment contained in four, interchangeable units.

Design equations and parity equations for multiple TDF gyros are derived using a projection matrix which greatly simplifies the mathematical manipulations. The existence of a failure isolation singularity for three TDF gyros is proved. The impact of this singularity on system design is shown through coverage calculations. Coverage of a second-gyro failure is calculated to be greater than 0.999999 for 1 deg/s or greater failure conditions, thus having very little impact on angle rate outputs to the FCS. Coverage for 1 deg/h failure criteria, however, can be as low as 0.99, and thus the singularity becomes a factor in net system failure probability of attitude or navigation outputs.

Test data of a representative redundant system show the feasibility of detection and isolation of small gyro and accelerometer errors in a nonvibrational environment. Angular misalignments between separated clusters of skewed, redundant inertial sensors can contribute significantly to contamination of this error detection process.

Acknowledgment

The preliminary redundant system design was performed under contract number NAS 1-13847 with NASA Langley Research Center. The test system used for the demonstration of redundancy management techniques was configured on a company IR&D program.

References

[1] "Preliminary Design of a Redundant Strapped Down Inertial Navigation Unit Using Two-Degree-of-Freedom Tuned-Gimbal Gyroscopes," Litton GCS, NASA CR-145305, Oct. 1976.

[2] Bjurman,B.E., Jenkins, G.M., Masreliez, C.J., McClellan, K.L., and Templeman, J.E., "Airborne Advanced Reconfigurable Computer System (ARCS)," Boeing Commercial Airplane Co., NASA CR-145024, Aug. 1976.

[3] Ebner, R.E., "Flight-Control/Navigation Inertial Reference System," National Aerospace and Electronics Conference,'77 *Record*, Dayton, Ohio, May 1977.